Effects of Laser Ablation on Aluminum Surface Condition and Ultrasonic Bond Interface Formation

Louis Castellanos[1], Maxwell Hein[2], Michael Brökelmann[2], Michael McKeown[1], Gina Kim[3]
[1]HESSE Mechatronics Inc., 10 Pasteur Street, Suite 100, Irvine, CA 92618, USA
[2]HESSE GmbH, Lise-Meitner-Str. 5, 33104 Paderborn, Germany
[3]University of California, Irvine, Irvine, CA 92697, USA
Email: Louis.Castellanos@Hesse-Mechatronics.com

Abstract
Laser ablation is increasingly being considered as a surface-preparation method for aluminum current collectors in electric-vehicle and aerospace battery manufacturing to improve wire bondability, first-pass yield, and reliability. However, conventional shear testing may not fully capture the quality of the bond interface on laser-processed surfaces. In this study, a Taguchi L9 orthogonal-array design of experiments was used to evaluate the effects of laser-ablation parameters on aluminum surfaces and subsequent wire bond formation. Bond performance was assessed through shear testing and microscopy-based surface characterization. Laser ablation generally increased the mean shear force relative to the isopropyl-alcohol-cleaned reference aluminum plate. However, selected conditions exhibited centrally unbonded regions over the most aggressively ablated areas despite maintaining comparatively high shear force. These findings demonstrate that laser ablation can improve bond quality but must be controlled within a validated process window.

Key words
Aluminum current collectors, bond-interface integrity, bond shear testing, laser ablation, surface morphology, ultrasonic wire bonding.

I. Introduction
Ultrasonic wire bonding is a solid-state joining process in which normal force and high-frequency motions create interfacial microslip, disrupt surface films, and develop intermetallic joining. The process is highly sensitive to the mechanical state of the mating surfaces because the oxide films must be displaced or fragmented before intimate metal-to-metal contact can develop [1], [2]. The same sensitivity also makes the process vulnerable to contamination, nonuniform native oxide, and surface conditions [3].
In general, the ultrasonic wire bonding process can be divided into four phases: pre-deformation and vibration activation, friction, ultrasonic softening and interdiffusion. The latter three phases overlap during the bonding process. The normal bonding force deforms the wire during the pre-deformation phase, creating an elliptical contact area between the wire and the substrate and causing cracks in the surface oxide layer [4]. Following ultrasonic activation, the wire begins to slide across the substrate, generating relative motion at the contact interface [5], [6]. The oxide layers within the contact region are detached from the metal surfaces and displaced toward the periphery or completely out of the contact area [3], [4], whereas the ultrasonic vibration induces a so-called ultrasonic softening effect, which promotes bulk deformation of the wire and deformation of the surface asperities [7], [8], [9], [10]. The bulk deformation further contributes to relative motion between the wire and the substrate, while asperity deformation increases the extent of intimate contact between the two surfaces. As local oxide layers are removed and fresh metal surfaces come into contact, microwelds are formed. Geissler et al reported this in a previous study, where a high-resolution transmission electron microscope captured local wire and substrate surfaces approaching approximately 3 nm [10]. This observation suggests that direct metallic bonding can occur once sufficiently close contact is achieved. However, owing to the continuing relative motion between substrate and wire, the formation of microwelds is accompanied by their deformation and eventual rupture, resulting in a continuous cycle of microweld formation, growth, and breakage during the bonding process [11].
Laser ablation offers a non-contact method to remove organic residue, modify oxide condition, and create repeatable surface texture before wire bonding. Recent studies on cylindrical battery cells have reported improved wedge-bond strength and more favorable failure modes after laser cleaning [12], [13]. However, the response does not follow a consistently increasing or decreasing trend. Excessive laser energy density can alter the surface morphology and cause substrate melting and additional oxidation [13], [14], producing surface conditions that may impede ultrasonic coupling.

The reliability consequence is important in high-current battery and power-electronic assemblies. Heavy wires and ribbons carry high current and are exposed to thermomechanical cycling, vibration, and local temperature changes. Traction-module studies identified bond-wire and interface degradation as contributors to power-cycling fatigue [15]. Other work has shown that heavy-ribbon bond strength depends strongly on the ultrasonic process window and that lift-off can persist even when strength appears adequate [16]. Qualification based only on a scalar shear threshold may therefore under-detect interface nonuniformity.

This paper has two purposes. First, it reports the available laser-ablation and bond-shear data for external technical review. Second, it identifies the controls and characterization required before claims about oxide phase, roughness, or calibrated laser fluence can be made.

The central hypothesis is that wire or ribbon bond strength depends on both surface chemistry and texture. After laser processing, a high shear force does not always indicate that the full intended area was successfully bonded.

II. Technical Background

A. Ultrasonic Interface Formation

The accepted sequence for ultrasonic bonding begins with tool loading and wire deformation, followed by relative motion at the interface. Harman describes bond development as a dynamic process in which friction and plastic flow expose fresh metal and expand the welded area [1]. G.G Harman and J. Albers further showed that ultrasonic deformation and interfacial slip are central to aluminum joining [2]. In practice, insufficient energy produces non-stick or bond lift-offs, whereas excessive force, time, or ultrasonic amplitude can overwork the wire, thin the heel, or damage the substrate [8].

B. Laser Surface Conditioning

A pulsed marking laser changes the surface through a combination of contaminant desorption, oxide disruption, and localized heating. The resulting surface condition is controlled not by a single parameter but by the combined effects of pulse energy, pulse frequency, pulse overlap, speed, and focal position. Because laser cleaning of aluminum operates within defined energy-density thresholds, relatively small changes in process conditions can shift the interaction from insufficient oxide removal to effective surface renewal or, at excessive settings, substrate melting and additional oxide formation [14].

Earlier laser-interconnection work for power devices likewise emphasizes reliability improvement as the primary rationale for modifying conventional thick-wire joining methods [17].

C. Shear Test Method

Wedge-bond shear testing is a destructive mechanical test used to evaluate the strength and quality of an ultrasonic wedge bond. A chisel-shaped shear tool is positioned close to the bond wire and pushed laterally against the side of the bond until the bond separates from the bonding surface. JESD22-B116B defines destructive bond shear as "a method for process development, process control, and quality assurance" [18]. The standard also cautions that wedge bonds have not been demonstrated to be a consistent indicator of bond integrity. The limitation is directly relevant to the present data: the shear measures the resultant force required to remove the bond, but the peak force can be carried by a perimeter or a subset of strongly welded regions. Post-shear image evaluation is therefore needed to determine whether the nominal bond footprint was included in the load transfer.

III. Experimental Method

A. Materials and Equipment

The study used 3003 aluminum plates, which are a commonly used alloy for busbars. Laser ablation was performed on a Keyence MD-X2520A marking system. Wire bonds were bonded on a Hesse Mechatronics BJ985 equipped with a 60 kHz HBK10 bond head using 500 µm Tanaka aluminum wire with a reported break-load range of 1,100 to 1,800 grams. Bond shear testing was measured using an XYZTEC Sigma system. Surface images and topographic measurements were collected using a Keyence VHX digital microscope. It should be noted that the VHX configuration was not a traceable stylus or interferometric roughness instrument; the reported areal parameters were treated as comparative rather than absolute metrology. Selected surfaces were also examined using a tabletop scanning electron microscope (SEM) TM3030Plus (Hitachi High-Tech Europa GmbH, Krefeld, Germany), with an energy dispersive X-ray spectrometer (EDS) Quantax 70 (Bruker Corporation, Billerica, MA, USA).

B. Laser Parameter Matrix

Four laser parameters were varied in a three-level Taguchi L9 orthogonal array: laser power, scan speed, pulse frequency, and line spacing. The baseline parameters, as shown in Table I, were based on the working settings established during system commissioning.

TABLE I. Laser Ablation Baseline Parameters

Baseline Parameters	
Power (%)	65
Scan speed (mm/s)	1500
Frequency (kHz)	120
Line Spacing (µm)	60
Spot Diameter (µm)	60

TABLE II. Laser ablation baseline parameters as the reference, and Taguchi L9 laser ablation parameter matrix, spot diameter is 60 µm for every trial.

Trial	Power in %	Speed in mm/s	Frequency in kHz	Spacing in µm
T1	45	1200	96	48
T2	45	1800	144	72
T3	45	1500	120	60
T4	85	1200	144	60
T5	85	1800	120	48
T6	85	1500	96	72
T7	65	1200	120	72
T8	65	1800	96	60
T9	65	1500	144	48

C. Bonding and Destructive Evaluation

Nine equal regions were marked on an aluminum plate, with one region assigned to each laser trial, as shown in Fig. 1.

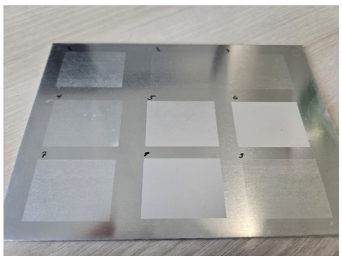


Fig. 1. Plate with laser ablated areas

A separate reference plate was cleaned with isopropyl alcohol and processed without laser treatment. Wire-bonding parameters were developed on the reference surface to produce stable results that met the requirements of the JESD22-B116 wire-bond shear test method. A total of 130 single bonds were bonded in each laser region, as shown in Fig. 2. Surface measurements and bond-process graphs were collected; pre-shear images were used to compare bond widths, and approximately 60% of the bonds in each region were randomly selected for destructive shear testing. Post-shear images were classified according to bonded-area remnants and the presence of central unbonded regions.

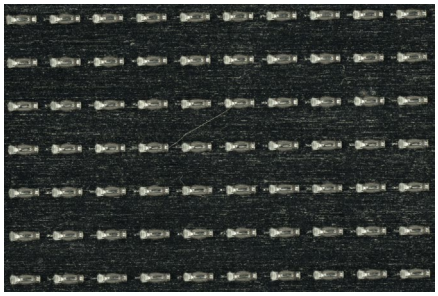


Fig 2. Example of a single bonded region; Trial 2

IV. Results

A. Chemical Characterization

The elemental composition of each sample was analyzed using EDX at a magnification of 1000x within a measurement area of approximately 170x120 µm². The oxygen concentration was subsequently normalized to the reference sample to enable a direct comparison between trials. As shown in Table II, the normalized oxygen concentration varies across the samples investigated, ranging from approximately 0.84 (Trial 7) to 1.48 (Trial 6). While most trials exhibit values close to the reference condition, several samples show elevated oxygen contents, indicating differences in the degree of surface oxidation induced by the respective process parameters. For surfaces that appear rougher to the eye, the oxygen content is also slightly higher, see Trials 1, 6, and 8 in Table III.

B. Process Results

Via the process integrated quality control, the bond-process data were collected. Fig. 3 presents the mean trajectories of the process-integrated monitoring signals obtained from the different trails, together with the corresponding ±1 standard deviation uncertainty range. The results are grouped by signal type and include current, deformation, frequency and sensor voltage.

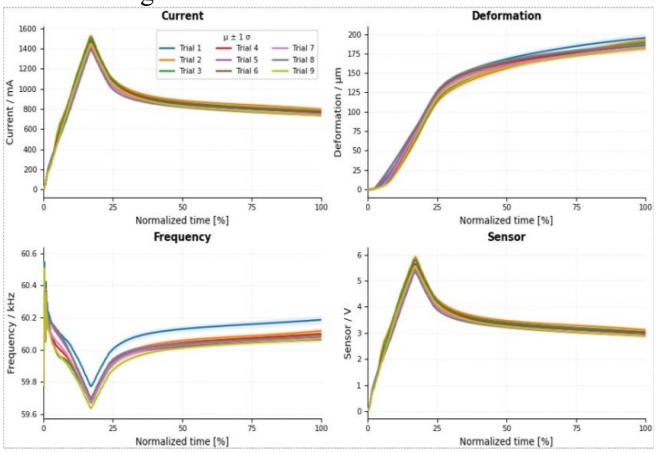


Fig. 3. Mean normalized current, deformation, frequency, and sensor signals from the trials. Shaded areas indicate the corresponding ±1 standard deviation range, demonstrating high signal repeatability and low variability across trials.

Across all test cases, the signals exhibit highly consistent behavior, indicating good process repeatability. The current and sensor signals show a pronounced peak during the initial phase of the process, followed by a gradual decay. In contrast, the deformation signal increases monotonically and approaches a plateau towards the end of the cycle. The frequency initially decreases, reaches a minimum during the transient phase, and subsequently recovers. The relatively small spread between the individual trials demonstrates that the measured process signatures are robust against the considered parameter variations, while the largest deviations occur during the dynamic phase of the process where the signal gradients are highest. These results show that the

different laser parameters for preparation of the aluminum surfaces are not reflected in the process data. Only trials 1 and 9 show slight deviations in the frequency

C. Shear Force

The isopropyl-alcohol-cleaned reference produced a mean shear force of 3.88 ± 0.13 kgf with a minimum of 3.47 kgf. All nine laser-processed conditions had mean values at or above the reference, as shown in Table III. Trial 4 was the strongest, with a mean of 4.25 ± 0.08 kgf and a minimum of 4.06 kgf. Relative to the reference plate, Trial 4 increased the mean force by 9.5% and the minimum force by 17.0%. Trial 9 produced a mean shear force that was effectively equal to the reference at the displayed precision.

TABLE III. Summary of Destructive Shear Results and oxygen concentration normalized to the reference

Trial	Min (kgf)	Avg ± SD (kgf)	Max (kgf)	Normalized Oxygen content
Ref.	3.47	3.88 ± 0.13	4.10	1.0
T1	3.90	4.20 ± 0.12	4.43	1.1
T2	3.82	4.01± 0.06	4.14	0.9
T3	3.90	4.13 ± 0.09	4.36	1.1
T4	4.06	4.25 ± 0.08	4.41	1.0
T5	3.78	4.02 ± 0.07	4.22	1.0
T6	3.92	4.12 ± 0.09	4.31	1.5
T7	3.76	4.08 ± 0.12	4.38	.8
T8	3.73	3.89 ± 0.07	4.04	1.3
T9	3.68	3.88 ± 0.10	4.15	1.0

condition, determined from EDX elemental analysis measurement with area of approximately 170x120 µm² at 1000x magnification.

D. Descriptive Main Effects

The mean responses for the power levels of 45%, 65%, and 85% were 4.11 ± 0.10, 3.95 ± 0.11, and 4.13 ± 0.12 kgf, respectively. The 1,200 mm/s level produced the highest mean response among the scan-speed levels at 4.18 ± 0.09 kgf, compared with 4.04 ± 0.14 kgf at 1,500 mm/s and 3.97 ± 0.07 kgf at 1,800 mm/s. The dominant screening trend was therefore poorer average strength at 1,800 mm/s, although the strongest individual condition combined high power, low scan speed, high frequency, and centerline spacing. The comparison of the mean responses for different process parameters is shown in Fig. 4.

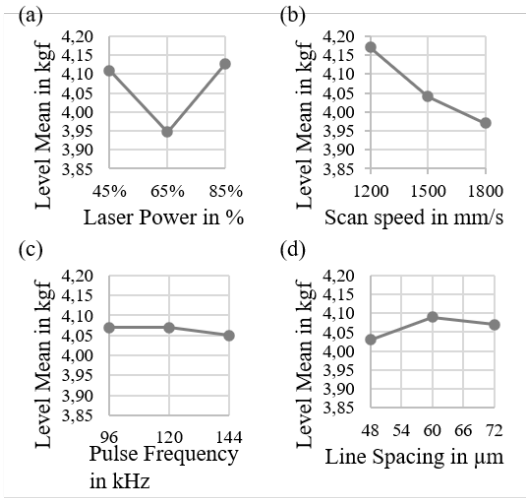


Fig. 4. Level Mean vs (a) Laser Power Setting, (b) Scan Speed, (c) pulse frequency, and (d) line spacing.

E. Surface Morphology and Roughness

The baseline aluminum plate retained parallel rolling marks and scattered surface contaminants. Trials 2, 3, 4, 7, and 9 also preserved the rolled texture and exhibited isolated or discontinuous resolidified features, which were consistent with limited pulse or line overlap. Trials 1 and 5 produced more regular chains of overlapping melt features, whereas Trials 6 and 8 generated the densest and most continuous bead-like tracks. The laser-induced features remained directionally aligned with the scan path, and the individual resolidified features in Trial 8 were visibly larger than those in Trial 6, as shown in Fig. 6.

The reported areal height parameters varied widely across the experiment. Sa ranged from 5.10 µm for the reference surface to 75.06 µm for Trial 7, while Sq ranged from 6.32 to 99.40 µm. However, visual morphology did not consistently correspond with the VHX-derived Sa and Sq values. Most notably, Trials 6 and 8 both exhibited the same localized central nonbonding morphology after shear, even though their reported Sa values were 10.14 and 48.32 µm, respectively, and their Sq values were 15.00 and 60.45 µm. Their skewness values also differed substantially, at -2.10 for Trial 6 and -0.67 for Trial 8. These results indicated that a single global amplitude parameter was insufficient to describe the surface features that governed bond-interface formation.

F. Interface Anomaly

Post-shear inspection identified a localized failure morphology that was not evident from the mean force alone. Trial 6 had 28 centrally unbonded regions, as shown in Fig. 6 (b), among 78 sheared bonds (35.9%), while Trial 8 had 23 centrally unbonded regions among 78 sheared bonds (29.5%), see Fig. 6 (c). The remaining seven conditions did not exhibit the same central unbonded regions morphology

within the reported sample, see Trial 3 in Fig. 6 (a) Trial 6 nevertheless had one of the highest mean shear values and a coefficient of variation of only 2.09%. Trial 8 had a lower mean value, but its coefficient variation (1.72%) was also lower than that of the reference. These observations demonstrated that a stable shear-force distribution could coexist with an undesirable interface geometry. Although Trials 6 and 8 exhibit contact areas that are not optimally bonded in the center beneath the wire, traces of microwelds, probably occurred during the ultrasonic bonding process according to Long et al., can be found, see white arrows in Fig. 6 (d) [11]. In addition to the aluminum residues, the deformed structure of the substrate is obvious, comparing the before and after impression of the surface in Fig. 5 (d) with Fig. 6 (d).

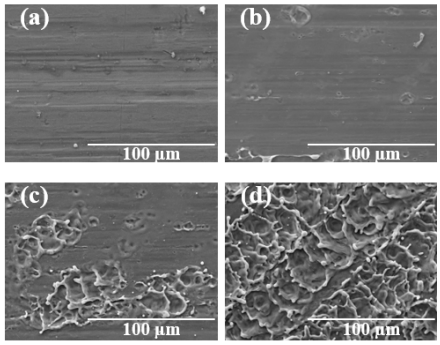


Fig. 5. SEM views at 1000x magnification show the transition from the (a) reference surface to weakly developed features in (b) Trial 3, (c) overlapping melt features for Trial 1, and (d) a dense laser-generated melt-track morphologies for Trial 6

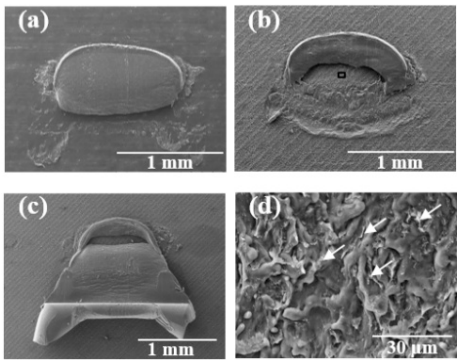


Fig. 6. Exemplary image of usual shear nuggets in (a) Trial 3, noteworthy shear nuggets in (b) Trial 6 and (c) Trial 8, (d) highlighted, black box from (b) showing shear area under bond in Trial 6, white arrows indicating microweld aluminum residues from the wire on the substrate forming ductile dimple-like fracture surfaces.

V. Discussion

A. Why Shear Force Could Mask Incomplete Bonding?

Peak shear force is a structural response of the bond, wire, and shear-tool geometry. It is not a direct measurement of the bonded area. A bond with a strong outer bonded area or several micro-welded spots could still withstand a high load before the last connected section finally breaks. If laser ablation generated a hard or chemically stable central film while leaving bondable material around the perimeter, the bond could produce a high force while still having reduced interface coverage. This interpretation was consistent with the observed combination of high average force and frequent central unbonded regions in Trial 6. Within these tests, no further investigations into the surface conditions (e.g. phases) or the topographic contact condition were carried out.

Local load concentration within a reduced bonded area could raise interfacial stress and have accelerated crack initiation under thermal-expansion mismatch, vibration, or current-induced heating. G. Coquery, R. Lallemand, D. Wagner, and P. Gibard, connected traction-module life expectancy to power thermal fatigue [15], and heavy-ribbon studies identified heel cracking and lift-off as process-dependent failure modes [16]. The present study did not include aging or power cycling and therefore could not quantify the potential reduction in service life. It did, however, establish a plausible screening indicator: the central unbonded area needed to be controlled before reliability testing should be performed.

B. Interpretation of the Laser Process Window

The results do not support a simple relationship in which greater laser input consistently produces higher bond strength. Trial 4 produced the highest mean shear force without the reported central unbonded regions. Trial 6 combined high power and low pulse frequency with the widest hatch spacing evaluated, 72 µm, whereas Trial 8 combined the lowest estimated pulse overlap with the intermediate hatch spacing level of 60 µm. Both conditions used the 96 kHz frequency level, but Trial 1 also used 96 kHz and did not exhibit the same morphology. This pattern suggests a coupled response involving local pulse energy, pulse overlap, line coverage, and potentially plate location. The L9 design efficiently screens main effects but cannot independently resolve these interactions.

The broader literature reported the same nonlinearity. A. Moghaddas and J. E. Gould observed improvement at lower cleaning intensity and degradation at higher intensity [13]. K. Bieliszczuk, J. Zręda, and T. M. Chmielewski, found that laser-cleaning parameters affected surface condition and joint quality on cylindrical cells [12]. F. Schneider et al. reported saturation-like behavior when laser heating was added during ultrasonic bonding [19]. Collectively, these studies supported defining an operating window using both mechanical and morphological criteria instead of selecting only the condition with the highest mean shear force.

C. Manufacturing Implications

For production implementation, laser ablation parameters should be qualified as a controlled process rather than

selected only from visual appearance or a single bond-strength result. Qualification should establish a repeatable process window for the primary laser variables, including laser power, scan speed, pulse frequency, and line spacing. Once qualified, these parameters should be locked within defined limits and managed through normal process-change control.

Qualification should evaluate both the condition of the laser-processed surface and the resulting bond performance. Attention should be given to conditions that produce acceptable average bond strength but show localized unbonded regions or visual abnormalities. These conditions may indicate that the process is operating near the edge of a stable manufacturing window.

A practical qualification should include repeated testing at the nominal laser setting and at selected upper and lower parameter limits to confirm that normal equipment and material variation does not cause the process to fall outside the acceptable bonding window.

Wire bonder machine process signals, such as ultrasonic current, deformation, frequency response, or other available sensor traces, may be useful for ongoing production monitoring. However, these signals should first be correlated with clearly classified destructive test results. For production control, destructive testing should therefore remain the primary method for establishing initial process capability, while surface inspection and machine-generated signals can be used as supplementary indicators for maintaining the qualified process.

A practical acceptance rule should therefore require all qualification criteria to be met simultaneously. The bond population should exceed the minimum force requirement, satisfy defined statistical requirements, and remain below an established limit for unbonded footprint area. This approach is consistent with the general principle that the wire, bonding tool, surface condition, and ultrasonic process settings should be optimized as a coupled system [20].

VI. Limitations and Future Work

The Taguchi L9 array was not independently replicated and therefore could not separate factor interactions, plate-to-plate variability, or day-to-day process variation from the estimated main effects. In addition, evaluating multiple conditions on a common plate may have introduced fixture-position, clamping, or plate-flatness effects.

SEM/EDS provided qualitative oxygen comparisons but did not identify oxide phase or film thickness, while the VHX-derived roughness measurements were comparative rather than traceable absolute measurements. Consequently, the proposed oxide condition and its relationship to the central unbonded morphology remained unconfirmed.

Future work will replicate the experiment across multiple plates and recorded sample locations. Traceable profilometry, cross-sectional analysis, and oxide-phase and thickness characterization will be used to evaluate the effects of laser overlap, surface chemistry, and microtopography. Additional substrate finishes, wire materials, and wire sizes will also be investigated.

VII. Conclusion

This study showed that laser ablation can improve ultrasonic wire bonding on aluminum, but the laser process must be qualified as more than a surface-cleaning step. All nine laser-treated conditions produced mean shear forces at or above the isopropyl-alcohol-cleaned reference. Trial 4 produced the strongest overall result, increasing the mean shear force by 9.5% and the minimum shear force by 17.0%.

Shear force alone, however, did not fully describe the condition of the bond interface. Trials 6 and 8 developed central unbonded regions in 35.9% and 29.5% of the inspected bonds, respectively, even though both produced relatively stable shear-force distributions. Trial 6 was especially important because it maintained a high average shear force despite the repeated interface anomaly. These results show that a bond can meet a mechanical strength requirement while still having incomplete bonded-area coverage.

For manufacturing qualification, laser parameters should therefore be selected using both mechanical performance and post-bond interface condition. A practical process window should consider shear force, variation within the bond population, bonded-area coverage, and failure morphology rather than relying on the highest average shear value alone. Further testing across multiple plates, material conditions, and repeated laser settings will be needed to determine the repeatability of the observed behavior and better define the effects of laser parameters, surface chemistry, and topography. The results provide a practical starting point for developing a controlled laser-ablation process for aluminum wire bonding while also showing why destructive testing and interface inspection should remain part of the qualification process.

Acknowledgment

The authors sincerely acknowledge Keiko Yamamuro of the Make a Difference Opportunity Program at the University of California, Irvine, for her assistance with experimental testing and data analysis and Mike Navar of Keyence Corporation for providing technical guidance on laser-ablation principles and process parameters.

References

[1] G. G. Harman, Wire Bonding in Microelectronics, 3rd ed. New York, NY, USA: McGraw-Hill, 2010.

[2] G. G. Harman and J. Albers, “The ultrasonic welding mechanism as applied to aluminum- and gold-wire bonding in microelectronics,” IEEE Trans. Parts, Hybrids, Packag., vol. PHP-13, no. 4, pp. 406–412, Dec. 1977.

[3] Y. Long, F. Dencker, A. Isaak, J. Hermsdorf, M. Wurz, and J. Twiefel, "Self-cleaning mechanisms in ultrasonic bonding of Al wire," Journal of Materials Processing Technology, vol. 258, pp. 58–66, 2018, doi: 10.1016/j.jmatprotec.2018.03.016.
[4] H. Gaul, M. Schneider-Ramelow, and H. Reichl, "Analysis of the friction processes in ultrasonic wedge/wedge-bonding," Microsystem Technologies, vol. 15, pp. 771–775, 2009, doi: 10.1007/s00542-009-0811-8.
[5] Y. Long, F. Schneider, C. Li, J. Hermsdorf, J. Twiefel, and J. Wallaschek, "Quantification of the energy flows during ultrasonic wire bonding under different process parameters," International Journal of Precision Engineering and Manufacturing-Green Technology, vol. 6, pp. 449–463, 2019, doi: 10.1007/s40684-019-00061-0.
[6] Y. Long, F. Dencker, A. Isaak, C. Li, F. Schneider, J. Hermsdorf, M. Wurz, J. Twiefel, and J. Wallaschek, "Revealing of ultrasonic wire bonding mechanisms via metal-glass bonding," Materials Science and Engineering: B, vol. 236, pp. 189–196, 2018, doi: 10.1016/j.mseb.2018.11.010.
[7] F. Blaha and B. Langenecker, "Dehnung von Zink-Kristallen unter Ultraschalleinwirkung," Die Naturwissenschaften, vol. 42, p. 556, 1955, doi: 10.1007/BF00623773.
[8] J. E. Krzanowski and N. Murdeshwar, "Deformation and bonding processes in aluminum ultrasonic wire wedge bonding," Journal of Electronic Materials, vol. 19, pp. 919–928, 1990, doi: 10.1007/BF02652917.
[9] U. Geissler, M. Schneider-Ramelow, and H. Reichl, "Hardening and softening in AlSi1 bond contacts during ultrasonic wire bonding," IEEE Transactions on Components and Packaging Technologies, vol. 32, pp. 794–799, 2009, doi: 10.1109/TCAPT.2008.2009930.
[10] U. Geissler, J. Funck, M. Schneider-Ramelow, H. J. Engelmann, I. Rooch, W. H. Müller, and H. Reichl, "Interface formation in the US wedge/wedge-bond process of AlSi1/CuNiAu contacts," Journal of Electronic Materials, vol. 40, pp. 239–246, 2011, doi: 10.1007/s11664-010-1439-2.
[11] Y. Long, B. He, W. Cui, Y. Ji, X. Zhuang, and J. Twiefel, "Investigations on the mechanism of microweld changes during ultrasonic wire bonding by molecular dynamics simulation," *Materials & Design*, vol. 192, Art. no. 108718, 2020, doi: 10.1016/j.matdes.2020.108718.
[12] K. Bieliszczuk, J. Zręda, and T. M. Chmielewski, "Influence of cylindrical cells surface cleaning by means of laser ablation on wedge wire bonding process," Coatings, vol. 14, no. 4, Art. no. 445, 2024, doi: 10.3390/coatings14040445.
[13] A. Moghaddas and J. E. Gould, "Application of laser cleaning in quality improvement of ultrasonic wire bonding process in battery pack assembly," in Proc. International Automotive Body Congress (IABC 2023), Livonia, MI, USA, 2023.
[14] J. Shao, R. Zhang, H. Dong, C. Cao, and S. Sun, "The energy density threshold evaluation for high-precision laser cleaning of the oxidized layer on 7075 aluminum alloy with 100 ns laser," International Journal of Advanced Manufacturing Technology, vol. 120, pp. 1901–1907, 2022, doi: 10.1007/s00170-022-08914-w.
[15] G. Coquery, R. Lallemand, D. Wagner, and P. Gibard, "Reliability of the 400A IGBT modules for traction converters: Contribution on the power thermal fatigue influence on life expectancy," in Proc. EPE'95, Sevilla, Spain, 1995, pp. 1060–1065.
[16] S. M. Park, S. Nagao, T. Sugahara, and K. Suganuma, "Heavy ribbon wire bonding for advanced power module packages," in Extended Abstracts of the 2013 International Conference on Solid State Devices and Materials, Fukuoka, Japan, 2013, pp. 480–481, doi: 10.7567/SSDM.2013.PS-14-15L.
[17] F. Kostrubiec, Z. Lisik, R. Pawlak, K. Jakubowska, and A. Korbicki, "New laser technology for wire bonding in power devices," Microelectron. J., vol. 32, nos. 5–6, pp. 543–546, 2001, doi: 10.1016/S0026-2692(01)00027-1.
[18] JEDEC Solid State Technology Association, Wire Bond Shear Test Method, JESD22-B116B, Apr. 2017.
[19] F. Schneider, Y. Long, H. Ohrdes, J. Twiefel, M. Brökelmann, M. Hunstig, A. Venkatesh, J. Hermsdorf, S. Kaierle, and L. Overmeyer, "Effect of laser assistance in ultrasonic copper wire bonding," in Proc. Lasers in Manufacturing Conference (LiM), Munich, Germany, 2017.
[20] C. W. Tok, I. Langut, A. Menache, D. R. M. Calpito, and Y. H. Chew, "Wire bonding improvement through optimal bonding tools and materials selection," in Proc. 9th Electronics Packaging Technology Conference, 2007, pp. 743–749, doi: 10.1109/EPTC.2007.4469785.